Packaging Technology of 2nd-Generation Aluminum Direct Liquid Cooling Module for Hybrid Vehicles

GOHARA, Hiromichi* SAITO, Takashi* YAMADA, Takafumi*

ABSTRACT

As activities for preventing global warming and allowing for effective use of resources, further improvements in the fuel efficiency of eco-friendly vehicles such as hybrid electric vehicles is called for. To that end, size and weight reduction of intelligent power modules (IPMs) for hybrid electric vehicles is required. To meet this need, Fuji Electric has developed three new packaging technologies: technology for designing a radiator with a structure capable of direct liquid cooling using aluminum, ultrasonic bonding technology and thermal resistance improvement technology that allows continuous operation at 175 °C. The 2nd-generation direct liquid cooling IPM using aluminum, which applies these technologies, has achieved a volume reduction of 30% and mass reduction of 60% from the 1st-generation model.

1. Introduction

Prevention of global warming and effective use of resources are gaining importance as shared activities by all the countries of the world. In the automotive industry, the development and dissemination of hybrid electric vehicles (HEVs) and electric vehicles (EVs) are accelerating. Inverter units, which are used for power control of these vehicles, are mounted in a limited space. They need to have a compact size and high degree of freedom for mounting, together with weight reduction and efficiency improvement in view of low fuel consumption. Power modules mounted in inverters also require size and weight reduction and efficiency improvement, and a size and weight reduction of 20% or more is desired for each generation. With in-vehicle power modules, in particular, efforts are underway to increase heat radiation using a direct liquid cooling structure and reduce weight with aluminum cooler.

Fuji Electric has developed an in-vehicle intelligent power module (IPM) with an aluminum direct liquid cooling structure that integrates inverters to control 2 motors and an buck-boost converter[1] to realize the high output required for HEVs. Figure 1 shows in-vehicle IPMs with an aluminum direct liquid cooling structure. The 2nd-generation IPM has achieved a volume reduction by 30% and mass reduction by 60% from the 1st-generation model[2].

This paper describes 3 packaging technologies applied to the 2nd-generation IPM: technology for designing a radiator with direct liquid cooling using aluminum, ultrasonic welding technology, and thermal resistance improvement technology that allows continuous operation at 175 °C.

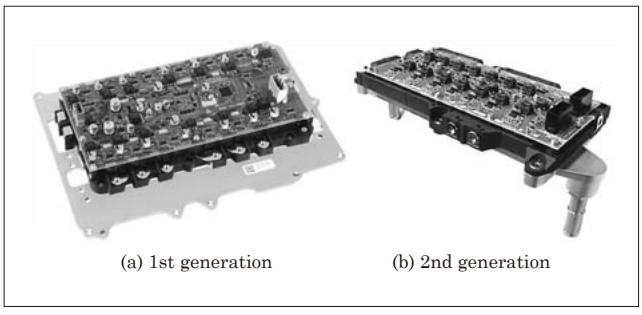

Fig.1 IPM with aluminum direct liquid cooling for automotive devices

2. Technological Issue with Cooling Structure

Figure 2 shows a cross-sectional structure of the 1st-generation IPM with aluminum direct liquid cooling. In this structure, the module and heat sink are bonded together directly by soldering.

The water jacket is designed independently by the user, which means that the heat sink and the water jacket are separate parts, and this requires a design process considering water-tightness and tolerance in

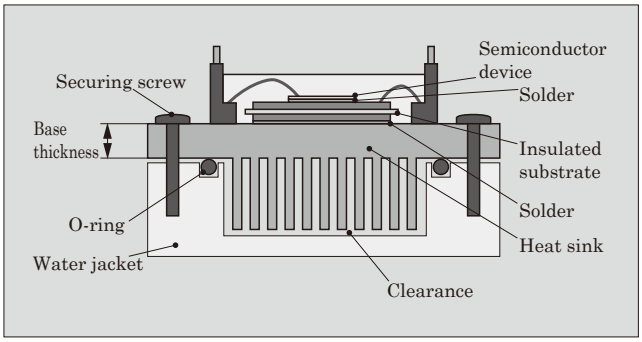

Fig.2 Cross-sectional structure of 1st-generation IPM with aluminum direct liquid cooling

* Corporate R&D Headquarters, Fuji Electric Co., Ltd.

addition to the flow channel design. For that reason, it is necessary to select materials and choose a base thickness in consideration of buckling and deformation, and this was a factor leading to an increase in thermal resistance.

In order to solve this issue and ensure improved heat radiation capacity and high reliability in the aluminum direct liquid cooling structure, we have developed an aluminum cooler integrating a heat sink and water jacket.

3. Cooler Designing Technology

3.1 Design of heat radiation performance

The heat radiation performance of a power module can be represented by 2 values: thermal resistance and thermal conductivity coefficient. Thermal resistance (R_{th}) is a value dividing the temperature difference between the chip junction and that of the point for comparison by the generated loss. Thermal conductivity coefficient (h) indicates the heat exchange performance of the coolant and fins. These relationships are represented by formula (1). It can be replaced by formula (2).

$$h = \frac{1}{R_{th} A} \quad \cdots\cdots(1)$$

h: Thermal conductivity coefficient [W/(m^2·K)]
R_{th}: Thermal resistance (K/W)
A: Fin surface area (m^2)

$$h = \frac{Nu\,\lambda}{L} \quad \cdots\cdots(2)$$

h: Thermal conductivity coefficient [W/(m^2·K)]
Nu: Nusselt number
λ: Thermal conductivity of component [W/(m·K)]
L: Fin representative length (m)

Nusselt number (Nu) can be calculated by formula (3) using geometry parameters. Here, Reynolds number (Re) can be represented by formula (4) and Prandtl number (Pr) by formula (5).

$$Nu = 0.664 Re^{1/2} Pr^{1/3} \quad \cdots\cdots(3)$$

Nu: Nusselt number
Re: Reynolds number
Pr: Prandtl number

$$Re = \frac{\rho v L}{\eta} \quad \cdots\cdots(4)$$

Re: Reynolds number
ρ: Density of coolant (kg/m^3)
v: Flow rate of coolant (m/s)
L: Fin representative length (m)
η: Viscosity of coolant (Pa·s)

$$Pr = \frac{\eta Cp}{\lambda} \quad \cdots\cdots(5)$$

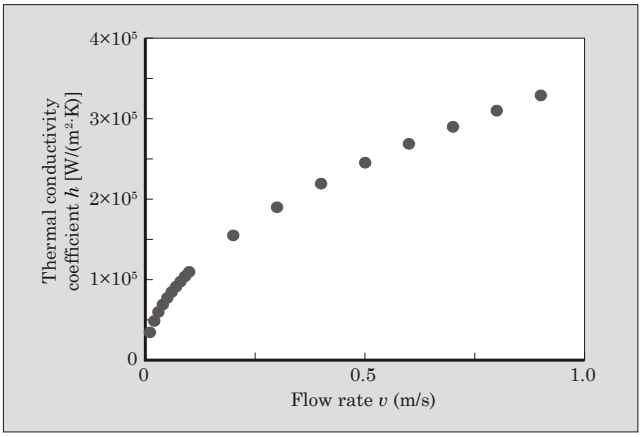

Fig.3 Relationship between thermal conductivity coefficient and coolant flow rate

Pr: Prandtl number
η: Viscosity of coolant (Pa·s)
Cp: Specific heat [J/(kg·K)]
λ: Thermal conductivity [W/(m·K)]

These formulas show that the thermal conductivity coefficient can be calculated from the density, viscosity, specific heat, thermal conductivity and flow rate of the coolant to be used. Figure 3 shows the thermal conductivity coefficient as functions of the flow rate calculated from the length per unit.

A higher fin surface flow rate provides a larger thermal conductivity coefficient that indicates the heat exchange performance. The heat generated in the chip is transmitted to the fins and radiated through the coolant, and the flow rate of the coolant on the fin surface has a significant impact on the heat radiation performance. Accordingly, improving the flow rate on the fin surface is the key point in heat radiation design[3].

3.2 Flow rate and heat radiation performance

With the conventional cooling structure that uses a sealing material, the water jacket is designed and prepared by the user; therefore, there is a need for tolerance design. This means that a clearance is required between the fin tips and the water jacket. We tentatively calculated the impact of this clearance on the heat radiation performance using a simplified model. The fins were shaped to have a thickness of 1 mm and height of 10 mm and arranged at intervals of 1 mm and the coolant was set to flow evenly into the coolant inlet at 1 L/min. Figure 4 shows the simplified model and simulation results.

It shows that a larger clearance caused the thermal resistance to increase and worsen. Because the coolant flows where the pressure resistance is low, it flows out in a wide clearance cross-sectional area, and the flow rate between the fins is reduced. In addition, parallel connection of modules is estimated to cause a significant reduction in the coolant flow rate.

It indicates that integrating the heat sink and water jacket to eliminate the clearance is effective in

increasing the coolant flow rate between fins and decreasing the thermal resistance.

Figure 5 shows a cross-sectional view of the new structure, which has been adopted as the 2nd-generation aluminum direct liquid cooling structure. In the new structure, the water jacket and fin tips have been bonded to eliminate the clearance. This has created a cooling structure that makes the most of the coolant. The portion that corresponds to the base has been made thinner and a high heat conductivity material has been used.

Figure 6 shows the result of comparing thermal resistances. The new structure takes into account the utilization of the coolant and thermal conductivity and is capable of reducing the thermal resistance by 20% from the conventional structure.

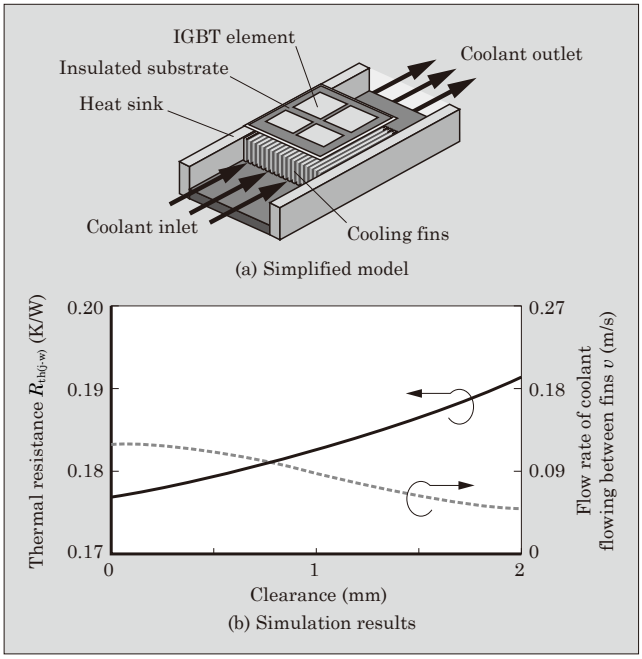

Fig.4 Simplified model and simulation results

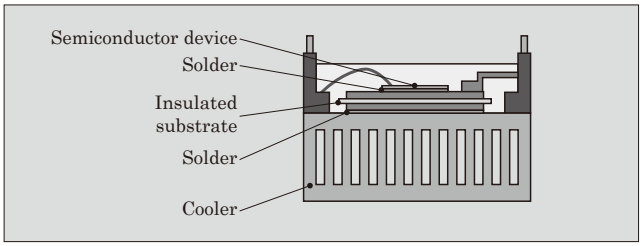

Fig.5 Cross-sectional structure of 2nd-generation IPM with aluminum direct liquid cooling

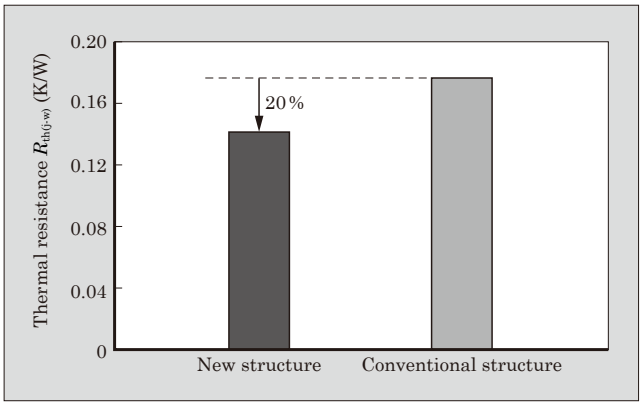

Fig.6 Thermal resistance

4. Ultrasonic Welding Technology

In the 1st-generation aluminum direct liquid cooling IPM, aluminum wire was used for connecting between the main terminals and internal circuit board. It required an area that allowed for the bonding of the number of wires required for ensuring the current density, and a large footprint according to the output was necessary for the wiring portion. To achieve size and weight reduction, the 2nd-generation IPM used ultrasonic welding for connection between the copper terminals, which are main terminals, and the internal circuit board. Figure 7 shows a photo of the appearance of the ultrasonic-welded copper terminals. Ultrasonic welding, in which copper terminals and a copper circuit of the board are directly bonded by solid-phase diffusion, offers secure bonding. Figure 8 shows a comparison between footprints of copper terminal ultrasonic welding and aluminum wire welding with the same current carrying capacity. By using direct welding of copper terminals, which have a higher conductivity

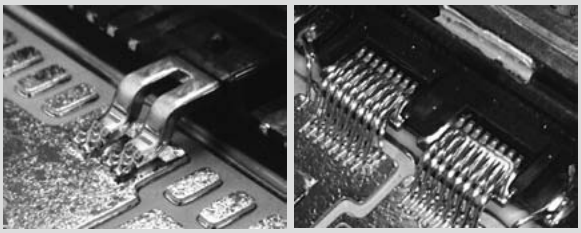

Fig.7 Appearance of welding

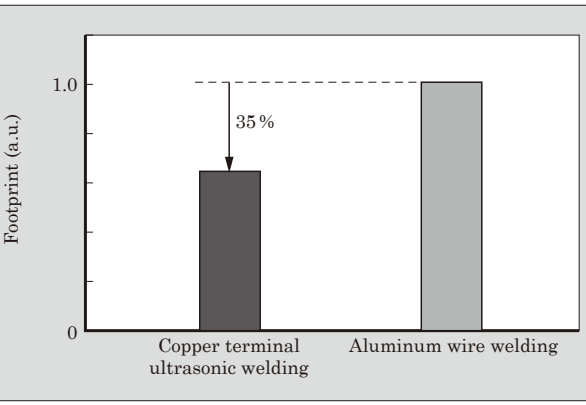

Fig.8 Footprint

than aluminum wire, the ultrasonic welding structure has achieved a footprint reduction by 35% from the aluminum wire welding structure.

The application of the ultrasonic welding technology, in addition to the improvement of heat radiation performance in the direct liquid cooling structure, has enabled the 2nd-generation aluminum direct liquid cooling IPM to realize a 30% volume reduction and 60% mass reduction from the 1st generation model.

5. Thermal Resistance Improvement Technology Allowing Continuous Operation at 175°C

The heat generated in the chip during IPM operation is radiated from the cooling fins through the baseplate. The upper limit of element temperature (T_j) is generally 150 °C. The maximized output in the range of ΔT, which is the difference between the water temperature and the element upper limit temperature, is determined. We aimed to achieve higher output by increasing the element guarantee upper limit T_{jmax} to 175 °C, in addition to reducing the thermal resistance.

To raise T_{jmax} from 150 °C to 175 °C, the impact of the element peripheral components on reliability must be improved[4]. We used the conventional module structure to conduct a power cycling test with T_{jmax} fixed. Figure 9 shows the test results. A temperature rise of 25 °C caused the lifetime to decrease by 40% with ΔT_j=75 °C.

Here, we focus on the lifetime decrease of the solder bond under the element. With the conventional Sn-Ag-based solder, strength degradation due to thermal deterioration is a possible factor causing the lifetime decrease. Next, we analyzed fracture modes and developed a new solder incorporating strengthening mechanisms to realize high thermal resistance and high strength.

5.1 Fracture modes of Sn-Ag-based solder

Figure 10 shows the result of observation of a cross section after the power cycling test. Cracks were observed along the grain boundaries of Sn. Sn-Ag-based solder has a structure that suppresses crack growth by strengthening grain boundaries with Ag_3Sn precipitating in Sn grain boundaries. However, heat generation in the soldered part and repeated stress due to the power cycling test brought about Ag_3Sn aggregation and Sn grain coarsening. This eliminated the grain boundary strengthening structure, which is a possible cause of the reduced lifetime. In particular, continuous operation at 175 °C causes the temperature of the solder bond directly under the chip to rise by approximately 25 °C as compared with operation at 150 °C. This accelerated the crack growth due to a change of the metallographic structure and thermal fatigue, apparently causing a lifetime decrease.

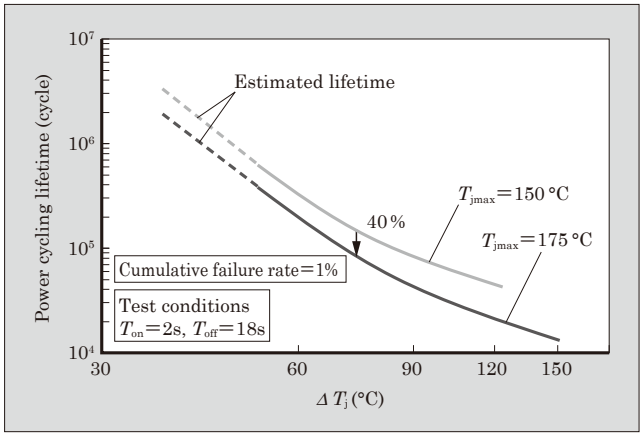

Fig.9 Power cycling lifetime decrease due to rise in T_{jmax}

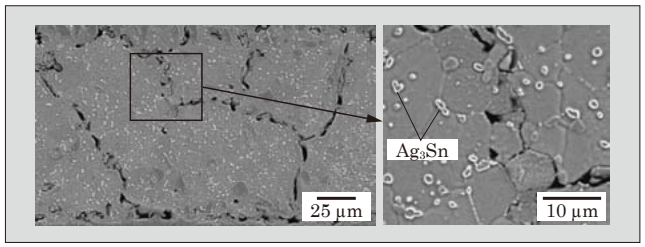

Fig.10 Power cycling lifetime decrease due to rise in T_{jmax}

5.2 Strengthening mechanism of solder

To develop a solder that does not change in the metallographic structure even in continuous operation at 175 °C and maintains the strength, we have focused on the strengthening mechanisms of metal materials. Typical strengthening mechanisms of solder include precipitation strengthening represented by Sn-Ag-based solder and solid solution strengthening with the addition of In or Sb[5]. Conventionally, either of the strengthening mechanisms was used for composition. However, in order to ensure reliability in continuous operation at 175 °C, we have added the third element with Sn-Sb-based solder used as the base. In this way, we have developed a new composite strengthening-type solder that combines the two strengthening mechanisms: precipitation strengthening and solid solution strengthening.

5.3 Mechanical characteristics of solder

Concerning the mechanical characteristics of the solder having both the precipitation and solid solution strengthening mechanisms, in order to examine the impact of strength degradation due to structural change under high temperature, we measured the tensile strength of samples subjected to aging* at room temperature and the high temperature of 175 °C for1,000 h. Figure 11 shows the results of measurement with an Sn-Ag-based solder, an Sn-Sb-based solder and the new solder.

The Sn-Ag-based solder showed a strength deg-

* Aging: A phenomenon in which metallic properties (for example hardness) change over time

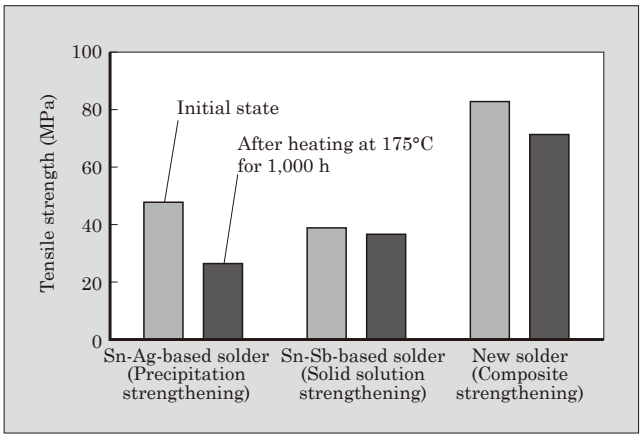

Fig.11 Tensile strength

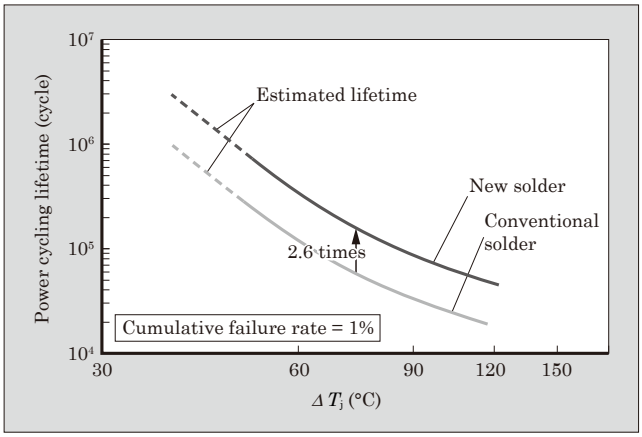

Fig.12 Results of power cycling test on new solder

radation of approximately 44% after heating at 175 °C for 1,000 h and the Sn-Sb-based solder, which has the solid solution strengthening mechanism, showed a strength degradation of approximately 5%. Meanwhile, the new solder with the composite strengthening mechanism showed a strength degradation of 13%. While the rate of strength degradation was somewhat high, the composite strengthening type features high strength in itself and raises expectations for improving the lifetime[6].

5.4 Results of power cycling test

To evaluate the reliability of the developed new solder at high temperature, we have conducted a power cycling test under the test condition of T_{jmax}=175 °C. Figure 12 shows the results of the power cycling test. As compared with the Sn-Ag-based solder, the new solder has been shown to have a power cycling lifetime that is 2.6 times longer at ΔT_j=75 °C.

6. Postscript

This paper has described packaging technologies for realizing size and weight reduction of IPMs for hybrid electric vehicles: technology for designing a radiator with a structure capable of direct liquid cooling using aluminum, ultrasonic welding technology and thermal resistance improvement technology that allows continuous operation at 175 °C.

Packaging technologies support customers with inverter development and design. We intend to use these technologies as the basis for working on further technological innovation to offer products that contribute to high efficiency and energy conservation.

References

(1) Gohara, H. et al. Packing Technology of IPMs for Hybrid Vehicles. FUJI ELECTRIC REVIEW. 2013, vol.59, no.4, p.235-240.
(2) Gohara, H. et al. “Next-gen IGBT module structure for hybrid vehicle with high cooling performance and high temperature operation”. Proceedings of PCIM Europe 2014, May 20-22, Nuremberg, p.1187-1194.
(3) Morozumi, A. et al. “Next-gen IGBT module structure for hybrid vehicle with high cooling performance and high temperature operation”. Proceedings of the 2014 IEEJ, Hiroshima, p.671-676.
(4) K, Vogel. et al. “IGBT with higher operation temperature- Power density, lifetime and impact on inverter design”. Proceedings of PCIM Europe, 2011, p.679-684.
(5) Saito, T. et al. “New assembly technologies for T_{jmax}=175°C continuous operation guaranty of IGBT module”. Proceedings of PCIM Europe 2013, Nuremberg, p.455-461.
(6) Saito, T. et al. “ Novel IGBT Module Design, Material and Reliability Technology for 175°C Continuous Operation”. Proceedings of IEEE 2014, Sep 14-18, Pittsburgh, p.4367- 4372.